LETTERS
PUBLISHED ONLINE: 19 AUGUST 2012 | DOI: 10.1038/NGEO1553

nature geoscience

Mantle flow deflected by interactions between subducted slabs and cratonic keels

Meghan S. Miller* and Thorsten W. Becker

Oceanic lithosphere is rapidly recycled into the mantle through subduction, an important part of the dynamic evolution of the Earth. Cratonic continental lithosphere, however, can exist for billions of years, moving coherently with the tectonic plates. At the Caribbean–South American Plate margin, a complex subduction system and continental transform fault is adjacent to the South American cratonic keel. Parallel to the transform fault plate boundary, an anomalous region of seismic anisotropy[1]—created when minerals become aligned during mantle flow—is observed[2–5]. This region of anisotropy has been attributed to stirring of the mantle by subducting slabs[2,3]. Here we use seismological measurements and global geodynamic models adapted to this unique region to investigate how mantle flow, induced by subduction beneath the Antilles volcanic arc, is influenced by the stiff, deep continental craton. We find that three components—a stiff cratonic keel, a weak asthenospheric layer beneath the oceans and an accurate representation of the subducted slabs globally—are required in the models to match the unusual observed seismic anisotropy in the southeast Caribbean region. We conclude that mantle flow near the plate boundary is deflected and enhanced by the keel of the South American craton, rather than by slab stirring.

The tectonic setting of the southeastern Caribbean involves subduction of oceanic lithosphere in opposite polarity beneath the Antilles arc and the Americas, which are linked by a transform plate boundary between continental South America and the Caribbean Plate (Fig. 1). The Cenozoic tectonic history has been primarily influenced by the Caribbean Plate migrating east relative to the Americas. About 55 million years (Myr) ago, the Caribbean Plate collided with both the Bahamas bank and northern South America[6] as it moved eastwards. The Caribbean Plate rotated clockwise as a result of to this collision, which initiated orogenesis in northern South America and development of the San Sebastian–El Pilar right lateral strike-slip system along the margin of northern South America to accommodate the sustained, east–west South American–Caribbean Plate motion[7]. Just a few hundred kilometres south of this complex plate boundary system lies the Guyana Shield, a ~1.7-billion-year-old craton, inferred to have a relatively rigid keel extending into the upper mantle (Fig. 1).

Data from broadband seismic instrumentation from temporary deployments and permanent national networks in Venezuela and in the surrounding region allow for the investigation of lithospheric and upper-mantle structure[8–10] beneath this complex plate boundary (Fig. 1). Rayleigh wave tomography[9] reveals a linear shear-wave velocity change that parallels the dextral strike-slip fault system along the northern coast of Venezuela, imaging the differences between the South American continental

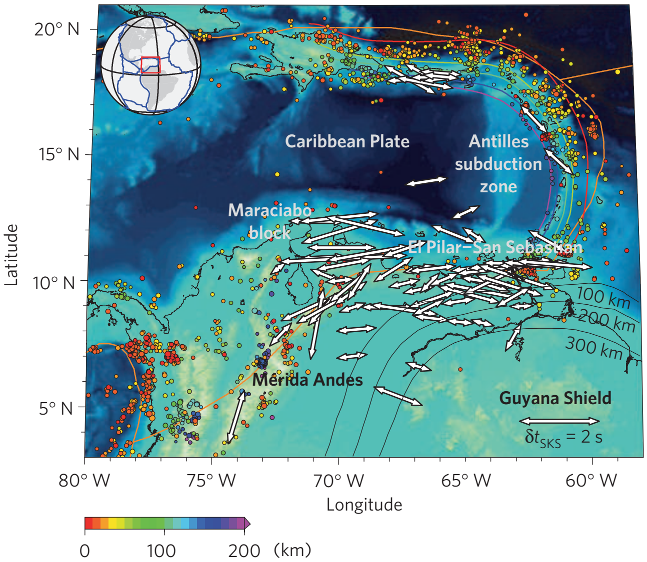

Figure 1 | Tectonic map of the southeastern Caribbean with shear-wave splitting measurements. Compilation of station-averaged SKS measurements[2–5]: white stick alignment shows apparent fast polarization orientation (fast azimuth), stick length scales with delay time δt_{SKS}. Coloured lines represent deep seismicity contours along the Antilles subduction zone[18] and black contours illustrate the position of the Guyana Shield (implemented as a high-viscosity region in our flow models, contours show domains with 100 times the upper-mantle background viscosity at the indicated depths). Dots are earthquakes (hypocentral depth (in km) colour coded)[30] and major plate boundaries are shown in orange.

lithosphere, the Venezuelan archipelago and the Caribbean oceanic lithosphere. The location of the Paria cluster earthquakes (<140 km; ref. 11), which are not associated with Benioff zone seismicity in northeastern Venezuela, steps in lithospheric and Moho depths across the plate boundary[9,12], and a low-velocity anomaly at the junction of the slab, transform boundary and craton[9] have led to the idea that the oceanic portion of the South American Plate is tearing away from the continental lithosphere as the westward-dipping subduction zone retreats eastwards along the northern margin of the continent[9,11].

Waveform-splitting analysis of core shear wave phases (SKS/SKKS) used to study seismic anisotropy[1] in the southeastern Caribbean[2–5] has found anomalously large delay times with fast polarization orientations parallel to the transform plate boundary. These 1.5–2.5 s shear-wave splits near the El Pilar–San Sebastian

Department of Earth Sciences, University of Southern California, 3651 Trousdale Parkway, Los Angeles, California 90089-0740, USA.
*e-mail: msmiller@usc.edu.

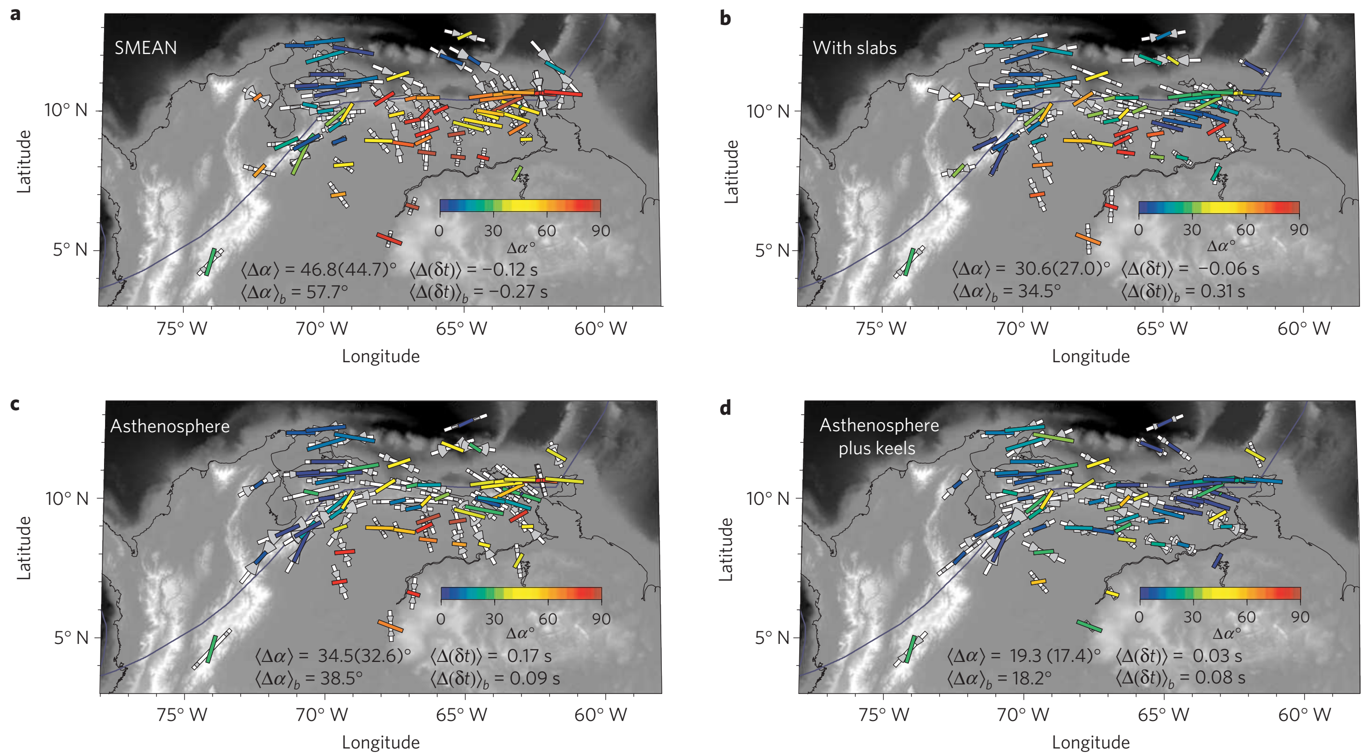

Figure 2 | Comparison of shear-wave splitting predictions and measurements. SKS splitting predictions (white sticks depicting delay time, grey wedges fast-azimuth variability with back-azimuth, ± one standard deviation), station-averaged splitting measurements are shown coloured by angular misfit. **a**, Results from the reference model using SMEAN (ref. 17). **b**, Reference model results plus inferred slab-density anomalies[18]. **c**, Model results with an additional asthenosphere layer beneath the oceanic lithosphere. **d**, Our best-fit model with the addition of deep continental keels. $\langle\Delta\alpha\rangle$ = mean azimuthal misfit (with quantities in parentheses weighted by delay time); $\langle\Delta(\delta t)\rangle$ = delay-time misfit for station, for station averages, $\langle\rangle$, and individual splits if back-azimuth information is available, $\langle\rangle_b$.

Fault, which marks the boundary between the Caribbean and South American plates (Fig. 1), are much larger in magnitude than the global average of ~1.0 s (ref. 13). However, the delay times decrease considerably (<1 s) away from the plate boundary towards the interior of the continent and the Guyana Shield. Large-magnitude splits in northern Venezuela have been interpreted as being associated with large-scale retrograde flow[2], which results from the Nazca Plate subducting beneath the South American Plate while the Nazca trench is retreating westwards. The motion of the Nazca slab would then lead to trench-parallel flow beneath it and the northern branch of this flow would be diverted eastwards below the Caribbean Plate. Later studies suggested that this eastward flow coupled with the eastward motion of the subducted oceanic lithosphere of the Antilles arc has created a strong vertical shear directly beneath the plate boundary[3,4].

The complex mantle structure and tectonic history of the region have been previously studied, but the interactions of the subduction zones, transform plate boundary and stiff continental keel are still poorly understood. We use high-resolution, global mantle flow models adapted for the seismically and geologically derived mantle and lithospheric structure of the Caribbean and South America, quantitatively predict shear-wave splitting from flow and compare the results with dense seismic observations to evaluate the influence of subducted slabs and cratonic keels on mantle convection and regional plate motions to test some of the dynamical questions of how the unusually strong seismic anisotropy has developed.

We ran 176 global geodynamic models to explore a range of viscosity (for example, weak asthenosphere, stiff keels) and density structures (for example, various slab morphologies, lithospheric structures) to evaluate which geodynamic scenarios are compatible with the observed anisotropy (Supplementary Figs S1 and S2). This approach provides for new quantitative testing of the tectonic relationships between the El Pilar–San Sebastian strike-slip system bounding the South American and Caribbean plates, the influence of the subducting slab beneath the Antilles arc and its possible detachment of the oceanic portion of the South American lithosphere from continental lithosphere. We model mantle circulation by solving the infinite Prandtl number, Stokes equation for incompressible fluid flow in a global, spherical shell[14,15] (see Methods and Supplementary Information). Density anomalies are inferred by scaling velocity anomalies from seismic tomography to temperature and all parameters, other than viscosity, are the same as those in ref. 16. Our reference model uses density anomalies derived from the SMEAN composite tomography model[17], but we also replace upper-mantle (cold/fast velocity) structure with subducting slabs (globally) inferred from Wadati–Benioff zone seismicity[18] and other seismicity-defined slab geometries (Supplementary Fig. S2). By computing global geodynamic models of mantle flow and inferred lattice preferred orientation (LPO) of olivine we are able to test and provide an explanation for the observed seismic anisotropy in the southeastern Caribbean. Although this modelling step from flow to LPO involves several uncertainties[19–22], we expect that the effect of density and viscosity variations will be dominant for the models considered here. Model performance is evaluated by comparing the real and synthetic splitting measures, for both station-averaged and back-azimuth specific splits, by computing the mean angular deviation of apparent fast polarization orientations (fast azimuths) $\Delta\alpha$ ($0 \leq \Delta\alpha \leq 90°$) and mean delay-time misfits $\Delta(\delta t) = \delta t_{\mathrm{model}} - \delta t_{\mathrm{data}}$.

Although we computed 176 global models, which are described in the Supplementary Information, we found three primary factors contribute to the best fit to the seismic anisotropy data. The reference model, based on SMEAN (ref. 17), predicts the splitting

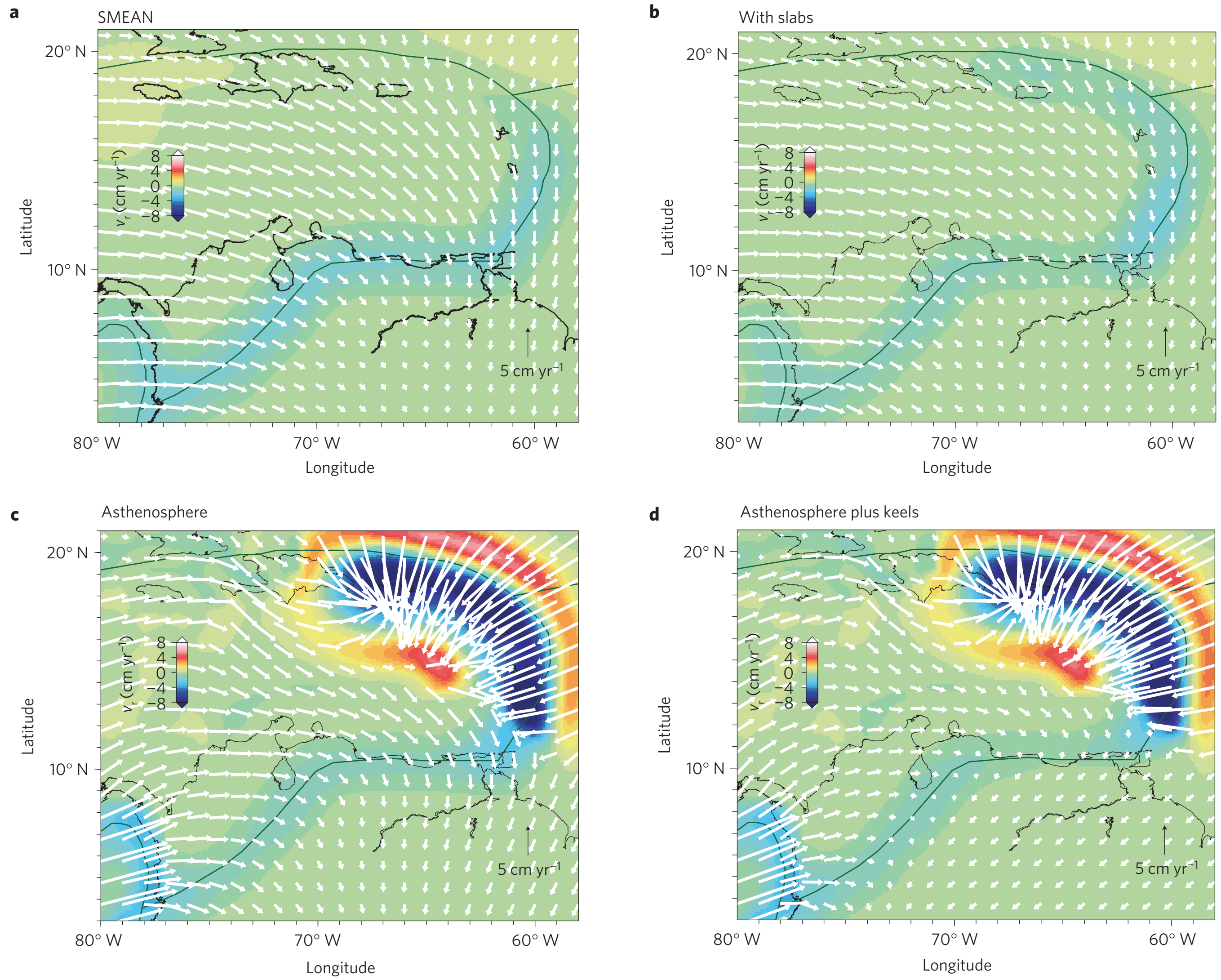

Figure 3 | Mantle flow models for the Caribbean–South America region. a–d, Flow generated at 165 km depth by the models shown in Fig. 2 with respect to fixed South America. Vectors are scaled by horizontal velocity and background colour represents the vertical velocity (v_r) with reds representing upward and blues downward flow, respectively. **d**, Flow for our best-fit model with an asthenospheric layer beneath the oceanic lithosphere and continental keels as described in the text.

orientations well at some stations near the plate boundary and in northwestern Venezuela, Mérida Andes and the Maracaibo block, but underpredicts delay-time magnitudes slightly (Fig. 2a). However, overall this model, without any adjustment for regional lateral viscosity variations, does not predict the decrease in magnitude or the orientation of the splitting measurements away from the plate boundary and into the interior of the South American continent or onto the Caribbean Plate. The second model (Fig. 2b) replaces the upper-mantle structure from tomography with slabs inferred from Benioff zone seismicity[18] because such models have been shown to lead to improvements in plate motion fits[23,24]. The third model (Fig. 2c) adds a weak, suboceanic asthenospheric layer to the global model (100–300 km depth, Supplementary Fig. S1). This model overpredicts the delay times for the shear-wave splits and degrades the fit for the stations in northeastern Venezuela (Fig. 2c), however it is an improvement from the SMEAN and slab model. Our preferred model is shown in Fig. 2d, which includes 300-km-deep keels based on cratonic geometry from Nataf and Ricard[25] to the global model with an asthenospheric layer at 100–300 km depths underneath all the oceans. Supplementary Fig. S2 illustrates the performance of all 176 models and the range of viscosity and density structures tested in terms of global velocity correlation, angular fast-orientation misfit and delay-time misfit. A range of robust misfit systematics exists for the various models. For example, the combination of cratonic keels and a weak asthenosphere beneath the oceanic plates always improves the match between the predicted and observed shear-wave splitting, as does implementation of lateral viscosity variations, compared with models without such effects. Specifically the addition of the cratonic keels globally, including the Guyana Shield to 300 km (Fig. 1), produces a stirring effect in the global model that overall markedly improves both the fast azimuth and delay-time misfit. The magnitude and orientation of the splitting predictions match the east–west-oriented measurements along both the plate boundary, the northeast–southwest-trending splits in the Maracaibo block and, more importantly, the smaller delay times that are measured in the continental interior and the craton, which none of the other ~160 models were able to do (see Supplementary Figs S2–S4).

Investigation of the calculated flow patterns at asthenospheric depths (165 km) illustrates the changes due to the lateral viscosity variations imposed in each of the four models described in Fig. 2. Adding the inferred slab structure produces only a very minor increase in velocity along the northern portion of the Antilles subduction zone and a slight decrease in velocities beneath the Caribbean Plate (Fig. 3a,b). However, the weak asthenosphere markedly increases the downward velocity of the subducting slab and flow around the edges of the plate. Yet, neither the orientation of flow along the South America–Caribbean Plate boundary nor beneath continental South America changes. With the addition of the stiff, deep continental keels into the global model the flow is deflected around and below the craton instead of into the interior of the continent (Fig. 3c,d). This deflection of flow around the craton improves the predicted splits beneath the cratonic continental lithosphere and improves the fit of the splits in northeastern Venezuela, while preserving the match to the observations in northwestern Venezuela. At greater mantle depths the flow returns to a generally north–south orientation. Although the Caribbean Plate motion is somewhat overpredicted, the surface-velocity orientations broadly match estimates based on geodetic data, providing insight into internal plate deformation and how plate velocities are affected by the stiff continental keel (Supplementary Figs S4 and S5).

When adapted to the expected lateral viscosity variations of the Caribbean and South America slab/craton system, our global models newly indicate a possible link to channelling of flow by the deep South American craton, where mantle is escaping around the southern end of the Antilles slab facilitated by a weak mantle wedge. Although our models are based on instantaneous-flow calculations, the anisotropic fabric is thought to have evolved into its preferred orientation over ∼10 Myr (see Supplementary Information). Therefore, we can assume that the present east–west velocity of the Caribbean Plate relative to stationary South America[7] has remained mostly constant during this timeframe and been a major factor in the development of the strong plate boundary parallel anisotropy. This supports the notion that the oceanic portion of the lithosphere is tearing away from continental South America. Intriguingly, it is not slab stirring[3] but the deep cratonic keel associated with the Guyana Shield that deflects and enhances mantle flow into a wide channel near the transform plate boundary from around the southern edge of the subducting slab. The keel acts as an anchor that decreases the overall surface velocity of South America, leads to increased internal deformation in the plate and contributes to the strong seismic anisotropy observed in the southeastern Caribbean.

Methods

We model mantle circulation by solving the infinite Prandtl number, Stokes equation for incompressible fluid flow (Boussinesq approximation) in a global, spherical shell[26,27]. We use a variant of the finite element code CitcomS[14,15] to arrive at steady-state solutions for density-driven flow using an approach similar to ref. 15 by prescribing plate boundaries as weak zones and solving for the resulting surface plate motions self-consistently. Our numerical resolution of ∼25 km laterally and vertically in the upper mantle allows us to resolve regional mantle flow at the required level of detail in a global model[16]. Density anomalies in the mantle are inferred by scaling the isotropic anomalies of a shear-wave velocity tomography model by a constant conversion factor $\mathrm{d}\ln\rho/\mathrm{d}\ln v_S = 0.2$, or by assigning constant density anomalies to upper-mantle slabs as inferred from the Wadati–Benioff zone geometry. All parameters, other than viscosity, are the same and discussed in ref. 16.

Seismic anisotropy, such as that measured most directly by shear-wave (SKS/SKKS) splitting, can be used to infer flow in the upper mantle because mantle rocks record deformation by means of the formation of LPO of olivine[13,28]. By computing geodynamic models of mantle flow and inferred LPO we can test possible explanations of the observed seismic anisotropy patterns. Both laboratory and field evidence show that the crystallographic axes of olivine align with shear and LPO development can be estimated quantitatively[20,28]. Synthetic LPO calculated for mantle flow models using kinematic LPO texturing theory[19] was benchmarked in ref. 21 to show that the synthetic LPO heterogeneity matches that observed in mantle xenoliths, implying that mineral physics methods and lab experiments may be valid when used for global applications. This is corroborated by a number of studies that have previously explored the link between flow and SKS splitting in simpler tectonic settings[22,29].

In our models, LPO is computed along streamlines as inferred from the instantaneous mantle flow solutions using the DREX method with parameters as discussed in ref. 19. We follow tracers in the mantle on forward advection until a logarithmic, finite strain of 0.75 is reached (typically within ∼10 Myr; ref. 21), assuming no feedback between seismic and mechanical anisotropy. Then from the LPO, seismic anisotropy is estimated by Voigt averaging single-crystal elastic tensors taking into account the depth-dependence of moduli[21]. Synthetic splitting is computed using a cross-correlation method from full waveforms that incorporate full anisotropy along the path and finite frequency effects[22], assuming an average 5° incidence angle. Model performance is then evaluated by comparison of the real and synthetic splitting measures by computing the absolute, angular deviation of fast apparent polarization direction (fast azimuths), ($0 \le \Delta\alpha \le 90°$), where $\Delta\alpha = 45°$ equal to the random mean and the delay-time misfit ($\Delta(\delta t) = \delta t_{\mathrm{model}} - \delta t_{\mathrm{data}}$), where $\Delta\delta t > 0$ indicates overprediction of anisotropy. Model performance is evaluated by comparing station-averaged splits with averages computed from full back-azimuth scans of synthetic waveforms, as well as split by split for the actual event back-azimuths if this information is available.

Received 1 November 2011; accepted 12 July 2012; published online 19 August 2012

References

1. Silver, P. G. & Chan, W. W. Implications for continental structure and evolution from seismic anisotropy. *Nature* **335,** 34–39 (1988).
2. Russo, R. M. & Silver, E. A. Trench-parallel flow beneath the Nazca Plate from seismic anisotropy. *Science* **263,** 1105–1111 (1994).
3. Russo, R. M., Silver, P. G., Franke, M., Ambeh, W. B. & James, D. E. Shear-wave splitting in northeast Venezuela, Trinidad, and the eastern Caribbean. *Phys. Earth Planet. Inter.* **95,** 251–275 (1996).
4. Growdon, M. A., Pavlis, G. L., Niu, F., Vernon, F. & Rendon, H. Constraints on mantle flow at the Caribbean–South American plate boundary inferred from shear wave splitting. *J. Geophys. Res.* **114,** B02303 (2009).
5. Masy, J., Niu, F., Levander, A. & Schmitz, M. Mantle flow beneath northwestern Venezuela: Seismic evidence for a deep origin of the Mérida Andes. *Earth Planet. Sci. Lett.* **305,** 396–404 (2011).
6. Pindell, J., Cande, S., Pitman, W. C., Rowley, K. C. & Dewey, J. F. A plate-kinematic framework for models of Caribbean evolution. *Tectonophysics* **155,** 121–138 (1988).
7. Perez, O. J. *et al.* Velocity field across the southern Caribbean plate boundary and estimates of Caribbean/South–American plate motion using GPS geodesy 1994–2000. *Geophys. Res. Lett.* **28,** 2987–2990 (2001).
8. Bezada, M. J., Levander, A. & Schmandt, B. Subduction in the southern Caribbean: Images from finite-frequency P wave tomography. *J. Geophys. Res.* **115,** B12333 (2010).
9. Miller, M. S., Levander, A., Niu, F. & Li, A. Upper mantle structure beneath the Caribbean–South American plate boundary from surface wave tomography. *J. Geophys. Res.* **114,** B01312 (2009).
10. Niu, F. *et al.* Receiver function study of the crustal structure of the southeastern Caribbean plate boundary. *J. Geophys. Res.* **112,** B11308 (2007).
11. Russo, R. M., Speed, R. C., Okal, E. A., Shepherd, J. B. & Rowley, K. C. Seismicity and tectonics of the southeastern Caribbean. *J. Geophys. Res* **98,** 14299–14319 (1993).
12. Clark, S. *et al.* Eastern Venezuelan tectonics driven by lithospheric tear geodynamics, not oblique collision. *Geochem. Geophys. Geosys.* **9,** Q11004 (2008).
13. Long, M. & Becker, T. W. Mantle dynamics and seismic anisotropy. *Earth Planet. Sci. Lett.* **297,** 341–354 (2010).
14. Moresi, L. N. & Solomatov, V. S. Numerical investigations of 2D convection with extremely large viscosity variations. *Phys. Fluid.* **7,** 2154–2162 (1995).
15. Zhong, S. J., Zuber, M. T., Moresi, L. & Gurnis, M. Role of temperature-dependent viscosity and surface plates in spherical shell models of mantle convection. *J. Geophys. Res.* **105,** 11063–11082 (2000).
16. Becker, T. W. & Faccenna, C. Mantle conveyor beneath the Tethyan collisional belt. *Earth Planet. Sci. Lett.* **310,** 453–461 (2011).
17. Becker, T. W. & Boschi, L. A comparison of tomographic and geodynamic mantle models. *Geochem. Geophys. Geosys.* **3,** Q1003 (2002).
18. Gudmundsson, O. & Sambridge, M. A regionalized upper mantle (RUM) seismic model. *J. Geophys. Res.* **103,** 7121–7136 (1998).
19. Kaminski, E., Ribe, N. M. & Browaeys, J. T. D-Rex, a program for calculation of seismic anisotropy due to crystal lattice preferred orientation in the convective upper mantle. *Geophys. J. Int.* **157,** 1–9 (2004).
20. Karato, S-i., Jung, H., Katayama, I. & Skemer, P. Geodynamic significance of seismic anisotropy of the upper mantle: New insights from laboratory studies. *Ann. Rev. Earth Planet. Sci.* **36,** 59–95 (2008).
21. Becker, T. W., Chevrot, S., Schulte-Pelkum, V. & Blackman, D. K. Statistical properties of seismic anisotropy predicted by upper mantle geodynamic models. *J. Geophys. Res.* **111,** B08309 (2006).
22. Becker, T. W., Schulte-Pelkum, V., Blackman, D. K., Kellogg, J. B. & O'Connell, R. J. Mantle flow under the western United States from shear wave splitting. *Earth Planet. Sci. Lett.* **247,** 235–251 (2006).

23. Ghosh, A., Becker, T. W. & Zhong, S. Effects of lateral viscosity variations on the geoid. *Geophys. Res. Lett.* **37,** L01301 (2010).
24. Stadler, G. *et al.* The dynamics of plate tectonics and mantle flow: From local to global scales. *Science* **329,** 1033–1038 (2010).
25. Nataf, H-C. & Ricard, Y. 3SMAC: An a priori tomographic model of the upper mantle based on geophysical modeling. *Phys. Earth Planet. Inter.* **95,** 101–122 (1996).
26. Hager, B. H. & O'Connell, R. J. A simple global model of plate dynamics and mantle convection. *J. Geophys. Res.* **86,** 4843–4867 (1981).
27. Ricard, Y. & Vigny, C. Mantle dynamics with induced plate tectonics. *J. Geophys. Res.* **94,** 17543–17559 (1989).
28. Ben Ismail, W. & Mainprice, D. An olivine fabric database: An overview of upper mantle fabrics and seismic anisotropy. *Tectonophysics* **296,** 145–157 (1998).
29. Fouch, M. J., Fischer, K. M., Parmentier, E. M. & Wysession, M. E. Shear wave splitting, continental keels, and patterns of mantle flow. *J. Geophys. Res.* **105,** 6255–6275 (2000).
30. Engdahl, E. R., van der Hilst, R. D. & Buland, R. Global teleseismic earthquake relocation with improved travel times and procedures for depth determination. *Bull. Seismol. Soc. Am.* **88,** 722–743 (1998).

Acknowledgements

M.S.M. was financially supported in part by EAR-1054638 and T.W.B. was financially supported in part by EAR-0643365. We thank A. Ghosh for assistance with assembling some of the density models, IRIS for providing the broadband seismic data and geodynamics.org and code contributors for maintaining CitcomS.

Author contributions

M.S.M. formulated the project. T.W.B. carried out numerical modelling. Both authors contributed equally to interpreting and analysing the data and to writing the paper.

Additional information

Supplementary information is available in the online version of the paper. Reprints and permissions information is available online at www.nature.com/reprints. Correspondence and requests for materials should be addressed to M.S.M.

Competing financial interests

The authors declare no competing financial interests.

nature geoscience | SUPPLEMENTARY INFORMATION
DOI: 10.1038/NGEO1553

Supplementary Material: Exploration of geodynamic model parameters, seismological measurements, and additional tectonic constraints

Viscosity structure of the four models shown in the main text

The global viscosity structure used for the four models whose seismic anisotropy and flow results are depicted in Figs. 2 and 3 is shown at asthenospheric (165 km) depth in Fig. S1. The reference model setup in Figure S1A is similar to that used in (refs. 1, 2) and based on scaling velocity anomalies from seismic tomography to temperature such that a constant scaling factor of $d \ln \rho / d \ln v_S = 0.2$ results. Figure S1b shows a merged model where we use the negative ("hot") anomalies from seismic tomography only, with slabs, as inferred from Wadati Benioff zones[3,4], serving to represent "cold" structure between the mantle depths of 100 and 660 km. The complete signal from tomography (including cold anomalies) is used in all other depth regions of the mantle.

This merged approach[1,5,6] is based on the recognition that global shear wave tomography models typically do not resolve subduction zone structure well, particular for the long-wavelength composite model SMEAN[7], which does, however, do a much better job than *P* wave models when evaluating plate driving forces[8,9] (see also Fig. S2e). Our computations include the effects of temperature on density and viscosity, via moderate temperature dependence as shown in Figure S1. Overall viscosity contrasts span ~four orders of magnitude, and lateral viscosity variations due to temperature alone are of order 10 to 100 for most models (we explore one case with larger variations). When combined with weak zones along plate boundaries, such models lead to good plate motion and geoid predictions in general[1,10]. As in Becker and Faccenna[2], our weak zones are assigned based on the NUVEL[11] plate boundaries, and consist of ~200 km wide zones where the viscosity of the lithosphere is reduced to 0.01 the background viscosity.

In terms of the resulting global viscosity fields (Fig. S1) in the asthenosphere, note the resulting prominent ridge structure, for example, in models a and b, leading to a moderately weaker mantle underneath the oceanic plates[12,13]. The further sub-oceanic viscosity reduction in case C that is prescribed as a factor 0.01 reduction within the depths of 100 and 300 km (as might be expected based on partial melt or high volatile content) and the relatively stiff keels in case D further emphasizes these ocean-continent contrasts.

Model dependence on density and viscosity structure

Figure S2 illustrates results for all of the 176 global flow models that were explored for this study in terms of their regional match to seismic anisotropy measurements and global plate motions. While a more complete parameter space exploration would be desirable, the computational efforts involved limited us to a somewhat restricted search, guided by our intuition as to which effects may be important by variation from the reference model that was based on prior modeling results. However, the resulting matrix of model performance in terms of plate motions and fit to seismic anisotropy yields a good impression of the importance of several parameters in density-viscosity structure space, and overall model robustness.

The rows in Figure S2 denote different viscosity models, from top to bottom:

V1. Reference viscosity structure, as in Figure S1a. Radial viscosity variations are limited to a higher viscosity lithosphere (0 to 100 km depth) and lower mantle (660 km to CMB, both increased by a factor of 50 compared to the upper mantle). Lateral viscosity variations include weak zones and inferred temperature dependent viscosity based on NUVEL[11] defined plate boundaries (see text and Figure S1a).

V2. Using Bird[14] plate boundaries for assigning weak zones rather than NUVEL[11].

V3. Addition of stiff keels to V1 for locations as inferred from 3SMAC[15] as in Figure S1d (see Figure 1 for detailed regional map of keel location).

V4. Addition of a sub-oceanic asthenospheric viscosity reduction to V1, similar to Figure S1c compared to S1b but using a smoothed oceanic-continent function, not capturing smaller plates such as the Caribbean.

V5. Combination of keels and asthenosphere as in V3 and V4.

V6. Sub-oceanic asthenosphere similar to V4 but sharp representation in all regions assigned as oceanic in 3SMAC[15], capturing Caribbean plate scale variations (as seen in Figure S1c).

V7. Addition of stiff keels for locations as inferred from 3SMAC[15] to V6.

V8. Like V7, but no temperature dependent lateral viscosity variations (i.e. only including lateral viscosity variations due to the asthenosphere and keels).

V9. Like V7, but stronger (~four orders of magnitude ridge to slab compared to ~2.5 for the reference) temperature dependent viscosity variations.

V10. Like V6, but modified oceanic asthenosphere structure around the southern end of the Antilles slab, allowing for a wider low viscosity gap between slab and keel.

V11. Addition of keels to V10.

The density structures used to define the rows of the matrices in Figure S2, going from left to right, are:

D1. Temperature anomalies inferred from RUM Wadati-Benioff zone contours[3] in the upper mantle (0 to 660 km) as used by Ghoshet al.[1], corresponding to 200 km-wide smooth slab density anomalies, with no tomography inferred anomalies.

D2. RUM inferred slabs[3] in the upper mantle as D1, but using a 150 km-wide, defined slab density anomaly.

D3. As D2, but downward continuation of the Caribbean slab (continuation of the seismicity contours shown in Figure 1 down to 660 km) based on Wadati-Benioff zone seismicity from the Engdahlet al.[16] catalogue.

D4. As D3, but additional "Colombian" slab, inferred to stretch northward from the Nazca plate underneath the Merida Andes (Figure 1) based on Wadati-Benioff zone seismicity from the Engdahl et al.[16] catalogue.

D5. Density in the mantle inferred from the global MIT *P* wave tomography model[17] (compare the discussion in Becker & Faccenna[2]).

D6. Upper mantle structure from the Widiyantoroet al.[18] regional *P* wave model, lower mantle inferred from SMEAN[7].

D7. Upper mantle structure from the global *SV* wave model by Lebedev and van der Hilst[19], lower mantle inferred from SMEAN[7].

D8. SMEAN[7] inferred temperature structure throughout the whole mantle.

D9. RUM inferred slabs[3] in upper mantle (0 – 660 km, as in D2), and SMEAN[7] tomography inferred structure in lower mantle.

D10. As D9, but additional extension of deep Caribbean slab as in D3.

D11. As D10, but additional “Colombia” slab as in D4.

D12. Slabs as in D1 and low velocity (“hot”) anomalies from SMEAN[7] in upper mantle, as used by Ghoshet al.[1].

D13. As model D12 but using full SMEAN[7] tomography for inferring temperature anomalies in the lithosphere (0-100 km) and in the lower mantle (660 km to CMB).

D14. As D12, but using the D2 RUM inferred slabs[3].

D15. As D14, but additional deep Caribbean slab as in D3 and D10

D16. As D14, but using the Syracuse and Abers[4]seismicity contours for global slab geometries.

Our discussion in the main text reflects the interpretation of the matrices shown in Figure S2. Based on the model performance for both fast orientations and delay times, as well as overall match to plate motions, we selected our four key models which build on density and viscosity structures based on the reference model as shown in Figures 2 and 3 as such: D8-V1 for the reference (Figure 2a), D13-V1 for the tomography/slab merged model (Fig. 2b), D13-V6 for the asthenospheric viscosity reduction (Fig. 2c), and D13-V7 for the addition of keels (Figure 2d); i.e. the progression of the viscosity structures in Figures 2b-d is based on one of the overall best-performing density models (Fig. S2).

Back-azimuth dependency of shear wave splitting measurements

The shear wave splitting measurements of apparent fast polarization orientation and delay time can be diagnostic of depth-variable or dipping anisotropy layers, and our method of computing synthetic splits from waveforms can make such back-azimuth specific predictions. We therefore also computed angular fast axes and delay time misfits (Figs. 2, S2b and d) for the subset of splitting data where event information was available[20,21]and for the models where our automated splitting based on the geodynamic predictions yielded a "good" split. This typically yielded ~60 data pairs, compared with the 66 pairs based on station-averaged (cf. Fig. 2). We found that, overall, back-azimuthal coverage of the available splitting data was insufficient to reliably establish any systematic and diagnostics of back-azimuth dependent splitting. Comparison of Figs. S2a-d shows that the back-azimuthally appropriate misfit shows similar model dependence on density and viscosity structure than the averaged approach. For some models, including our best-fit model, the misfits are slightly reduced for individual splits compared to the averaged approach, but this is not true for all of the models considered. Given these results, we mainly discuss station-averaged comparisons in the main text.

Anisotropy prediction match to more northerly arc regions

In our analysis of the relationship between seismic anisotropy and mantle flow in the subduction zone/craton environment in northeastern South America in the main text we focused on the transform fault setting away from the actual Antilles subduction zone. Figure S3a provides the wider scale context for the whole region of Figure 1 in terms of the match of measured *SKS* splitting to our model predictions. It is apparent that the Caribbean island station measurements with mainly trench orthogonal apparent fast axes are not fit well by our flow model, and we attribute this to the well known complexities of shear wave splitting in the mantle wedge region above subduction zones (e.g. role of water and complex 3D flow for local dynamics and LPO formation, see, e.g., reviews [22,23]) which we cannot consistently address with our current model setup. Alternatively, these mismatches may also be attributed to anisotropy from fabric within or below the slab, as can be inferred from local *S* splitting analysis for a few stations along the arc [24].

Deep mantle flow patterns

The main text discusses the role of the mantle keel in deflecting flow downward and therefore matching anisotropy in the southern portion of the study area much better (Fig. 2). Figure S4 illustrates how the predicted mantle velocities change throughout the upper mantle for the models shown in Figures 2c and d. The layer at 165 km (shown in Figure 3 for all four models) shows the effect of the keel most clearly; with a keel, mantle velocities are overall reduced and the southward flow found for model depths of 165 and 435 km is deflected deeper and only seen around 425 km for the keel model.

Crustal velocity predictions and GPS geodesy

Figure S5 compares the surface velocities for the four models of Figures 2 and 3 with the motions in the region as seen in geodesy. We have compiled campaign and network data from studies[25-29] and show all results in a best-fit, South American plate fixed reference frame. The overall convergence style of the region is matched well for our flow models, particularly for the model including a keel, but Caribbean plate motion amplitudes are overpredicted. Since oceanic plate motion is highly sensitive to the underlying asthenospheric viscosity [30,31], the fit to plate motions could likely be improved by fine-tuning the viscosity structure. However, we refrain from such optimization here.

References

[1] Ghosh, A., Becker, T.W., &Zhong, S., Effects of lateral viscosity variations on the geoid. *Geophys. Res. Lett.*37, L01301, (2010).

[2] Becker, T.W. &Faccenna, C., Mantle conveyor beneath the Tethyan collisional belt. *Earth Planet. Sci. Lett. 310*, 453-461 (2011).

[3] Gudmundsson, O. &Sambridge, M., A regionalized upper mantle (RUM) seismic model. *J. Geophys. Res. 103*, 7121-7136 (1998).

[4] Syracuse, E.M. &Abers, G.A., Global compilation of variations in slab depth beneath arc volcanoes and implications. *Geochem. Geophys. Geosys.*7 (2006).

[5] Yoshida, S. &Nakakuki, T., Effects on the long-wavelength geoid anomaly of lateral viscosity variations caused by stiff subducting slabs, weak plate margins and lower mantle rheology. *Phys. Earth Planet. Inter.172*, 278–288 (2009).

[6] Stadler, G., Gurnis, M., Burstedde, C., Wilcox, L. C., Alisic, L. &Ghattas, O. The dynamics of plate tectonics and mantle flow: from local to global scales, *Science 329*, 1033-1038 (2010).

[7] Becker, T.W. &Boschi, L., A comparison of tomographic and geodynamic mantle models. *Geochem. Geophys. Geosys. 3*, Q1003 (2002).

[8] Steinberger, B. & Calderwood, A., Models of large-scale viscous flow in the Earth's mantle with constraints from mineral physics and surface observations. *Geophys. J. Int. 167*, 1461-1481 (2006).

[9] Becker, T.W. & O'Connell, R.J., Predicting plate velocities with mantle circulation models. *Geochem. Geophys. Geosys. 2*, Q1060 (2001).

[10] Zhong, S.J., Zuber, M.T., Moresi, L., &Gurnis, M., Role of temperature-dependent viscosity and surface plates in spherical shell models of mantle convection. *J. Geophys. Res. 105*, 11,063-11,082 (2000).

[11] DeMets, C., Gordon, R.G., Argus, D.F., & Stein, S., Current plate motions. *Geophys. J. Int.* 101, 425-478 (1990).

[12] Becker, T.W., On the effect of temperature and strain-rate viscosity on global mantle flow, net rotation, and driving forces. *Geophys. J. Int.* 167, 943-957 (2006).

[13] Cadek, O. &Fleitout, L., Effect of lateral viscosity variations in the top 300 km on the geoid and dynamic topography. *Geophys. J. Int.*152, 566-580 (2003).

[14] Bird, P., An updated digital model of plate boundaries. *Geochem. Geophys. Geosys.* 4, Q1027 (2003).

[15] Nataf, H.-C. and Ricard, Y., 3SMAC: An *a priori* tomographic model of the upper mantle based on geophysical modeling. *Phys. Earth Planet.Int.* 95, 101-122 (1996).

[16] Engdahl, E.R., van der Hilst, R.D., &Buland, R., Global teleseismic earthquake relocation with improved travel times and procedures for depth determination. *Bull. Seismo. Soc. Amer.* 88, 722-743 (1998).

[17] Li, C., van der Hilst, R.D., Engdahl, E.R., & Burdick, S., A new global model for P wave speed variations in Earth's mantle. *Geochem. Geophys. Geosys.* 9, Q05018 (2008).

18. Widiyantoro, S., Kennett, B.L.N., & van der Hilst, R.D., Seismic tomography with P and S data reveals lateral variations in the rigidity of deep slabs. *Earth Planet. Sci. Lett.* 173, 91-100 (1999).

19. Lebedev, S. & van der Hilst, R.D., Global upper-mantle tomography with the automated multimode inversion of surface and S-wave forms. *Geophys. J. Int.* 173, 505-518 (2008).

20. Russo, R.M., Silver, P.G., Franke, M., Ambeh, W.B., & James, D.E., Shear-wave splitting in northeast Venezuela, Trinidad, and the eastern Caribbean. *Phys. Earth Planet.Inter.* 95, 251-275 (1996).

21. Growdon, M.A., Pavlis, G.L., Niu, F., Vernon, F., &Rendon, H., Constraints on mantle flow at the Caribbean-South American plate boundary inferred from shear wave splitting. *J. Geophys. Res.* 114, B02303 (2009).

22. Long, M. & Becker, T.W., Mantle dynamics and seismic anisotropy. *Earth Planet. Sci. Lett.* 297, 341-354 (2010).

23. Karato, S.-i. and Jung, H. and Katayama, I. and Skemer, P. Geodynamic signficance of seismic anisotropy of the upper mantle: new insights from laboratory studies. *Ann Rev. Earth Planet. Sci.* 36, 59-95 (2008).

24. Piñero-Feliciangeli, L.T. and Kendall, J.-M. Sub-slab mantle flow parallel to the Caribbean plate boundaries: Inferences from SKS splitting. *Tectonophys*. 462, 22-34 (2008).

25. Jouanne, F., Audemard, F., Beck, C., van Welden, A., Ollarves, R., &Reinoz, C., Present-day deformation along the El Pilar Fault in eastern Venezuela: Evidence of creep along a major transform boundary. *J. Geodyn.* 51, 398-410 (2011).

[26] Perez, O.J., Bilham, R., Bendick, R., Velandia, J.R., Hernandez, N., Moncayo, C., Hoyer, M., &Kozuch, M., Veloccity field across the southern Caribbean plate boundary and estimates of Caribbean/South-American plate motion using GPS geodesy 1994-2000. *Geophys. Res. Lett.* 28, 2987-2990 (2001).

[27] Perez, O.J., Bilham, R., Sequera, M., Moncayo, C., Rodreguez, C., Velandia, J.R., Guzman, M., & Molnar, P., Campo de velocidades GPS en el occidente de Venezuela: Componente lateral derechaasociada a la falla de Boconocomponenteconvergente perpendicular a los Andes. *Interciencia*36, 39-44 (2011).

[28] Trenkamp, R., Kellogg, J.N., Freymueller, J.T., & Mora, H.P., Wide plate margin deformation, southern Central America and northwestern South America, CASA GPS observations. *J. S. Amer. Earth Sci.* 15, 157-171 (2002).

[29] Weber, J.C., Dixon, T.H., DeMets, C., Ambeh, W.B., Jansma, P., Mattioli, G., Saleh, J., Sella, G., Bilham, R., & Perez, O.J., GPS estimate of relatvie motion between the Caribbean and South American plates, and geological implications for Trinidad and Venezuela. *Geology* 29, 75-78 (2001).

[30] Becker, T.W., On the effect of temperature and strain-rate viscosity on global mantle flow, net rotation, and driving forces. *Geophys. J. Int.* 167, 943-957 (2006).

[31] Gerault, M., Becker, T.W., Kaus, B.J.K., Faccenna, L., Moresi, L.N., &Husson, L., The role of slabs and oceanic plate geometry for the net rotation of the lithosphere, trench motions, and slab return flow. *Geochem. Geophys. Geosys.*13, Q04011 (2012).

Supplementary figure captions

Figure S1: **Maps of global viscosity structure**. Viscosity variation maps at asthenospheric (165 km) depth for the four models discussed in the main text (Figs. 2 and 3), colored by the $\log_{10}$ of viscosity, η, normalized by the upper mantle viscosity, $\eta_{um,}$, equal to 10^{21} Pas.

Figure S2: **Model performance matrices**. Regional (**a** and **b)** (as in Fig. 2) angular orientation misfit for fast apparent polarization axes ("fast azimuth") for *SKS* splitting, **c** and **d**, regional delay time misfit, and, **e**, global plate velocity correlation for all of the 176 global flow models considered. Plots **a** and**c** use station averaged splitting measurements and synthetics and **b** and **d** use event back-azimuth information for actual, non-averaged splits when available for measurements and synthetics. See text for density and viscosity model explanations.

Figure S3: **Comparison of shear-wave splitting predictions and measurements.** Larger scale *SKS* splitting **a**, compared to the regional subset considered for the analysis in the main text **b**, (identical to Figure 2**d**). Anisotropy predictions are plotted as white lines with gray wedges depicting the fast-azimuth variability with back-azimuth for each station, oriented with the mean fast azimuth. The colored lines show station-averaged splitting measurements at each station colored by model to measurement misfit (as in Fig. 2). $\Delta\alpha$ = azimuthal misfit; $\Delta(\delta t)$ = delay time misfit with $\langle\rangle$ indicating average of all **a,** 77 and **b,** 66 stations, station-averaged.

Figure S4: **Mantle flow models for the Caribbean-South America region.** Mantle flow generated at depths of **a & d,** 75, **b & e,** 165, and **c & f,** 435 km for models corresponding to Figures 2**c** and 2**d** respectively, in a South American plate fixed reference frame. The vectors are scaled by velocity amplitude and the color background represents the vertical velocity with red for upward, and blues for downward flow, respectively, as in Figure 3 (see legends for scales).

Figure S5: **Predicted surface plate velocities.** Predicted velocities for the models, **a-d**, shown in Figures 2 and 3 (orange vectors) compared to our compilation of GPS estimates[25-29] of crustal motions calculated plate motion vectors (blue vectors, for reference see text), all in a South America plate fixed reference frame (note significant intraplate deformation for some of the geodynamic flow models).

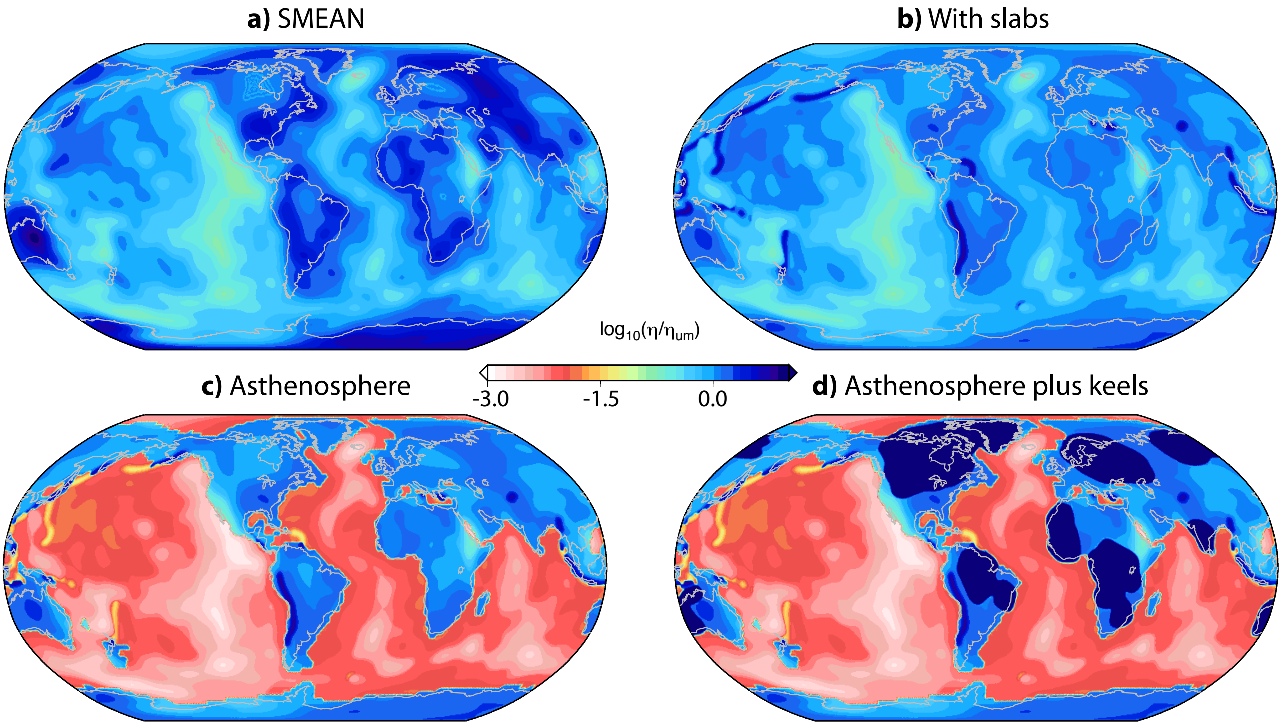

a) SMEAN
b) With slabs
log10(η/ηum)
-3.0
-1.5
0.0
c) Asthenosphere
d) Asthenosphere plus keels

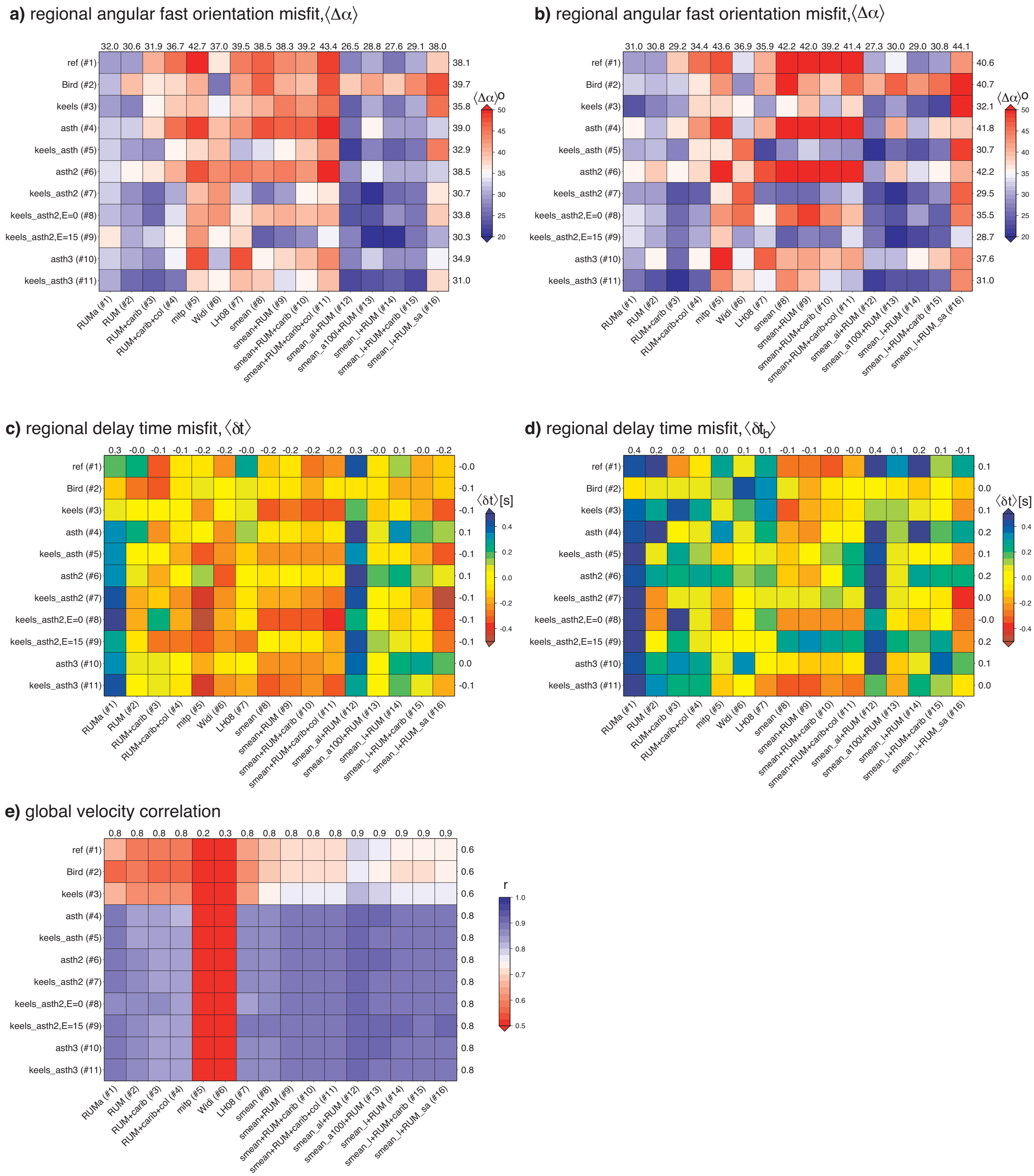
a) regional angular fast orientation misfit, ⟨Δα⟩
b) regional angular fast orientation misfit, ⟨Δα⟩
c) regional delay time misfit, ⟨δt⟩
d) regional delay time misfit, ⟨δt_b⟩
e) global velocity correlation
ref (#1)
Bird (#2)
keels (#3)
asth (#4)
keels_asth (#5)
asth2 (#6)
keels_asth2 (#7)
keels_asth2,E=0 (#8)
keels_asth2,E=15 (#9)
asth3 (#10)
keels_asth3 (#11)
RUMa (#1)
RUM (#2)
RUM+carib (#3)
RUM+carib+col (#4)
mitp (#5)
Widi (#6)
LH08 (#7)
smean (#8)
smean+RUM (#9)
smean+RUM+carib (#10)
smean+RUM+carib+col (#11)
smean_al+RUM (#12)
smean_a100l+RUM (#13)
smean_l+RUM (#14)
smean_l+RUM+carib (#15)
smean_l+RUM_sa (#16)
⟨Δα⟩o
⟨δt⟩[s]
r

a)

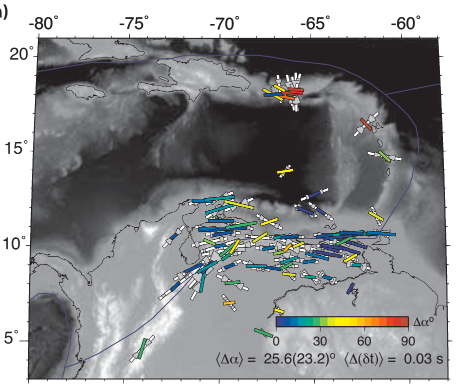
-80°
-75°
-70°
-65°
-60°
20°
15°
10°
5°
Δα°
0
30
60
90
⟨Δα⟩ = 25.6(23.2)° ⟨Δ(δt)⟩ = 0.03 s

b)

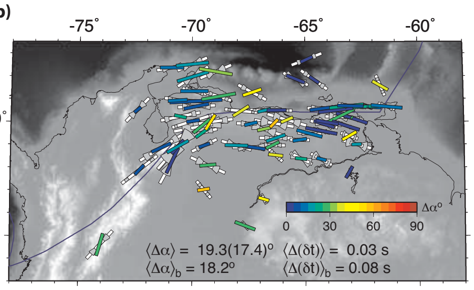
-75°
-70°
-65°
-60°
10°
5°
Δα°
0
30
60
90
⟨Δα⟩ = 19.3(17.4)° ⟨Δ(δt)⟩ = 0.03 s
⟨Δα⟩b = 18.2° ⟨Δ(δt)⟩b = 0.08 s

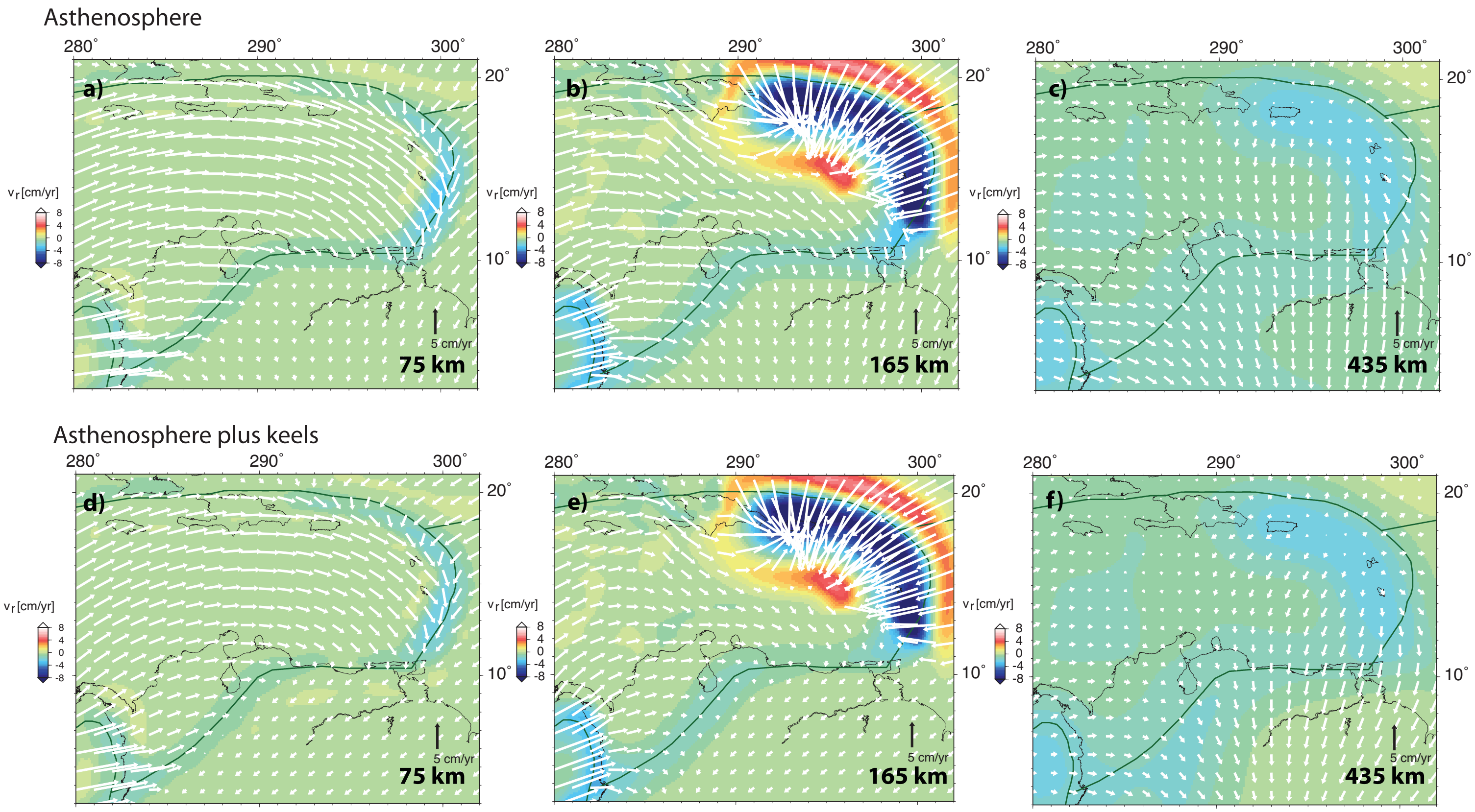
Asthenosphere
Asthenosphere plus keels
280°
290°
300°
20°
10°
a)
b)
c)
d)
e)
f)
v_r [cm/yr]
8
4
0
-4
-8
5 cm/yr
75 km
165 km
435 km

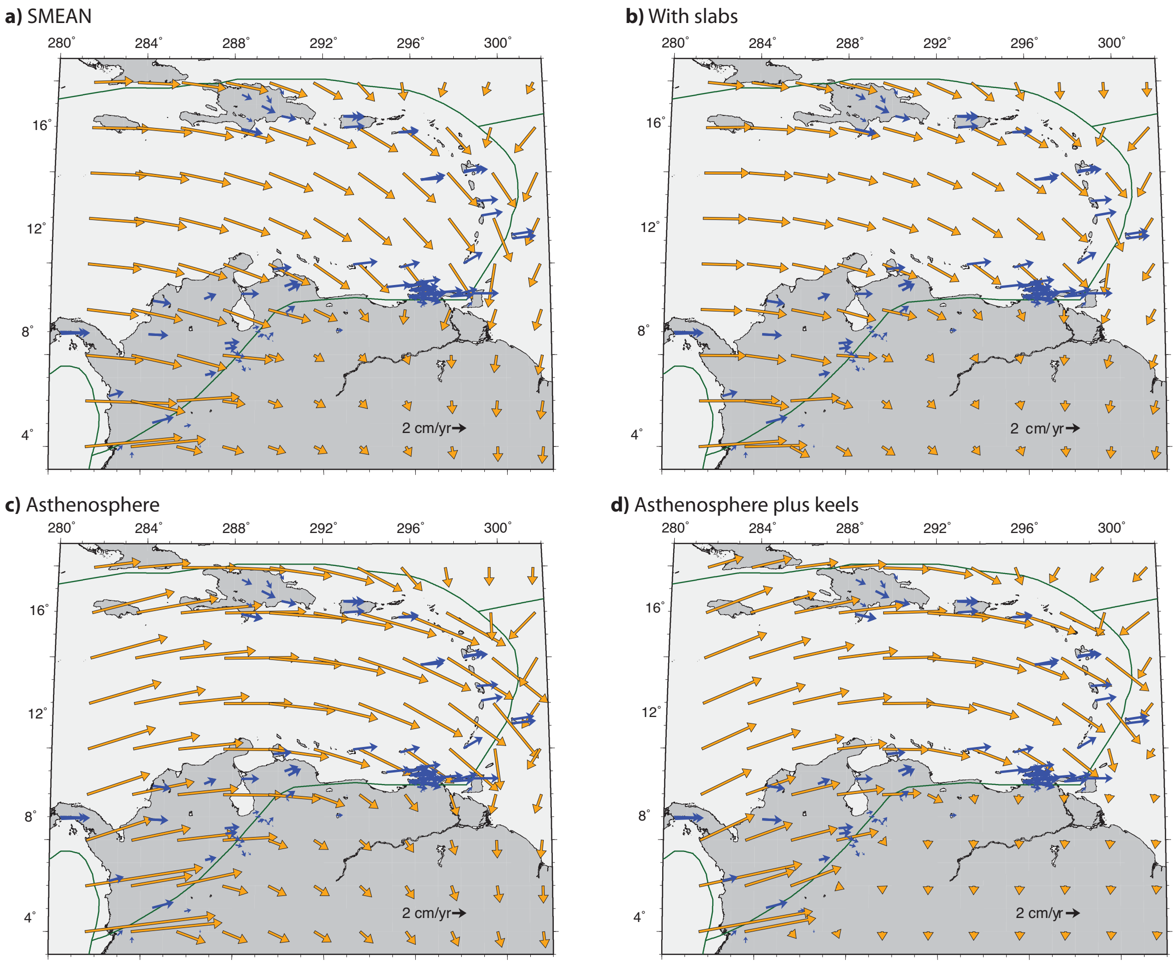
a) SMEAN
b) With slabs
c) Asthenosphere
d) Asthenosphere plus keels
280°
284°
288°
292°
296°
300°
16°
12°
8°
4°
2 cm/yr